8-16-2019

Computational and Experimental Approach to Understanding the Structural Interplay of Self-Assembled End-Terminated Alkanethiolates on Gold Surfaces

Juganta K. Roy
Jackson State University

Erick S. Vasquez
University of Dayton, evasquez1@udayton.edu

Henry P. Pinto
Jackson State University

Swati Kumari
Mississippi State University

Keisha B. Walters
University of Oklahoma

Follow this and additional works at: https://ecommons.udayton.edu/cme_fac_pub

Part of the Other Chemical Engineering Commons, and the Other Materials Science and Engineering Commons

See next page for additional authors

Author(s)

Juganta K. Roy, Erick S. Vasquez, Henry P. Pinto, Swati Kumari, Keisha B. Walters, and Jerzy Leszcynski

ARTICLE

Computational and Experimental Approach to Understanding the Structural Interplay of Self-assembled End-terminated Alkanethiolates on Gold Surfaces

Juganta K. Roy[1], Erick S. Vasquez[2], Henry P. Pinto[1,3], Swati Kumari[4], Keisha B. Walters[5*] and Jerzy Leszczynski[1*]

Applications of self-assembled monolayers (SAMs) on surfaces are prevalent in modern technologies and drives the need for a better understanding of the surface domain architecture of SAMs. To explore structural interaction at the interface between gold surfaces and a hydroxyl-terminated alkanethiol, 11-hydroxy-1-undecanethiol, (C11TH) we have employed a combined computational and experimental approach. Density functional theory (DFT) calculations were carried out on the thiol-gold interface using both the Perdew–Burke-Ernzerhof (PBE) and van der Waals (optB86b) density functionals. Our *ab initio* molecular dynamics (AIMD) simulations revealed that the interface consists of four different distinguished phases, each with different C11TH orientations. Experiments involved deposition of C11TH SAMs onto gold, with the resultant surfaces examined with X-ray photoelectron spectroscopy (XPS) and ellipsometry. Weighted average projected density of states (PDOS) of the different phases were photoionization cross section corrected and these were confirmed by experimental XPS data. Computed molecular parameters including tilt angles and the thickness of SAMs also agreed with the XPS and ellipsometry results. Hydrogen bonding arising from the terminal hydroxyl groups is the primary factor governing the stability of the four phases. Experimental results from XPS and ellipsometry along with DFT simulation results provide insights into the formation of the different orientations of SAM on Au(111) which will guide future efforts in the self-assembled SAMs architecture for other thiols or metal substrates.

Introduction

Self-assembled monolayers (SAMs) on metal surfaces play a pivotal role in modern surface chemistry with broad applications ranging from biosensors to electronics to catalysis in part due to the easy adaptability and inherent binding preferences of SAMs[1–7]. Specifically, end-terminated alkanethiolates with longer chain lengths self-assembled on gold (Au) surfaces common and serve as a representative system for a wide variety of SAMs. The effect of van der Waals (vdW) [8–10] and π-π stacking interactions[11–13] are key aspects of the self-assembly process in order to understand how to improve the formation, stability and performance of SAMs of the devices utilizing thiol-Au SAMs.

The mechanism of SAM formation on Au(111) surfaces via gold adatom moieties (RS−Au$_{ad}$−SR) for saturation coverage is well

understood[14-16]. A considerable number of experimental studies have been published addressing the Au-S interaction to determine the thiol anchored self-assembly mechanisms[17,18]. Besides, the Au-S interaction, the final structure formed through self-assembly is that which is most energetically favorable via balancing multiple types of interactions such as vdW forces, electrostatic forces and hydrogen bonding[19]. Although vdW forces are weak in comparison to the short-range chemical bonds, their cumulative effect can play a decisive role in molecular conformation and orientation which impacts the lattice parameter[20], electronic properties[21], and stability of organic/inorganic interfaces[3,22]. It is known that many self-assembly phenomena are enhanced directly by non-covalent interactions[23–25]. Therefore, to gain a better understanding and more accurate prediction of SAMs properties, DFT calculations need to include van der Waals density functional (vdW-DF) and be validated by experimental evidence. The focus of this work is the chemisorption of the thiols via gold adatom configurations, as this is a stable model for longer alkanethiol SAMs on Au(111) surfaces[16,25].

A considerable number of investigations on SAMs have examined end-functionalized alkanethiols [HS-(CH$_2$)$_n$-G] on Au (111) substrate as a prototype of the self-assembly process, where G is (non-alkane) terminal functional group. It is well known that the presence of end-functionalized group, such as -COOH, -NH$_2$, or -OH, on an alkanethiol significantly affects the SAMs structure and the resultant surface properties[26,27]. In this work, the electronic structure of an -OH terminated alkanethiol, C11TH on an Au (111)

[1]*Interdisciplinary Center for Nanotoxicity, Department of Chemistry, Physics and Atmospheric Sciences, Jackson State University, Jackson, MS 39207, USA*
[2]*Department of Chemical and Materials Engineering, University of Dayton, Dayton, OH 45469-0256, USA*
[3]*School of Physical Sciences and Nanotechnology, Yachay Tech University, 100119 Urcuqui, Ecuador*
[4]*Swalm School of Chemical Engineering, Mississippi State University, MS State, Mississippi 39762, USA*
[5]*School of Chemical, Biological and Materials Engineering, The University of Oklahoma, Norman, OK 73019, USA*
Corresponding author: Prof. Keisha Walters, Phone: +1 405 325 0465; fax: +1 405 325 5813; E-mail: keisha.walters@ou.edu
Prof. Jerzy Leszczynski, Phone: +1 601 979 3723; fax: +1 601 979 7823; E-mail: jerzy@icnanotox.org

substrate is investigated. Numerous theoretical calculations, such as density functional theory (DFT)[28–32] and classical molecular dynamics[33], have been performed to understand the alkanethiol SAM assembly process-both with and without terminal functional groups-but most did not include the vdW interactions[24]. In the literature, a considerable number of DFT studies have examined the methane thiolates as a model system but very few reports exist for the longer alkanethiols[30,34–39]. In order to accurately describe the SAM structures that arise for longer chain alkanethiols, theoretical studies need to be more realistic and consider the vdW interactions. Some prior approaches take into account the vdW dispersion include PW91[37,40,41], GGA-PBE-D2[38], GGA-PBE-TS[38], and opB86b-vdW[38,42]; the latter effort revealed that including vdW dispersion correction not only changes the adsorption energy by ca. 30-40%, it also results in a structure that is in better agreement with the experimental results[42].

Within this context, our objective in the present work is to gain a complete understanding of the morphology, electronic structures, and energetics of the Au(111)/C11TH interface. X-ray photoelectron spectroscopy (XPS) and ellipsometry were used to examine the interfaces experimentally along with DFT calculations that include PBE and vdW-DF functionals. These combined methods provide results that present new molecular-level insight into the Au(111)/C11TH interface and could have significant implications within the broad field of material science with applications ranging from molecular electronics to drug delivery technologies.

2 Materials and methods

2.1 Experimental details

Ethanol (200 proof) and 11-hydroxy-1-undecanethiol (C11TH, 99%) were used as received and obtained from Sigma-Aldrich and used as received. SAM deposition on Au substrates was performed by placing 10 mm × 10 mm gold-coated flat silicon wafers [Au(111) coated Si, Platypus Technologies] in C11TH/ethanol solutions for 24 h. After SAM deposition, the wafer was rinsed three times in clean ethanol and dried under a nitrogen stream. The wafers were characterized immediately after SAM deposition to avoid any possible contamination.

Ellipsometry data was collected using a variable angle spectroscopy ellipsometer (VASE) with a wavelength range of 245 – 1000 nm (M2000, Woollam Co.). A Cauchy layer model with a refractive index of 1.48 was used for SAM thickness fitting analysis. XPS data was collected using a PHI 1600 XPS electron scanning chemical analysis instrument equipped with a PHI 10-360 spherical detector. An achromatic Mg Kα X-Ray source was used operating at 300 W and 15 kV. XPS data was collected with PHI surface analysis software (version 3.0) at either a pass energy of 23.8 eV at a 55° angle of incidence or 187.8 eV at a 45° angle of incidence. A total of 45 scans were collected and averaged for each sample. A binding energy range of 0-20 eV was used with a step size of 0.2 eV. Results from both the ellipsometry and XPS data were compared with the simulated data.

2.2 Computational details

Calculations of the interface of end-terminated alkanethiol (C11TH) and gold surface were performed using the plane-wave based Vienna *ab initio* simulation package (VASP)[43,44] implementing density functional theory (DFT) and the generalized gradient approximation (GGA) of Perdew-Burke-Ernzerhof (PBE)[45] functional and van der Waals density functional (vdW-DF) optB86b as implemented by Klimeš, Bowler and Michaelides[46,47]. It is essential to mention that conventional DFT has no description of nonlocal electron-electron correlations (dispersion forces) and therefore is unable to describe the physisorption of molecules on surfaces accurately. The core electrons for Au-[Xe]4f14, C[He], O-1s2 and S-[Ne] are described by the projected augmented wave (PAW)[48]; that includes scalar-relativistic corrections for the Au atom. The Au(111)/C11TH interface was modelled considering the widely accepted $c(4\times2)$ supercell structure consisting of four C11THs with full coverage[14,28,49] and four layers of Au atoms with a vacuum (in the *z*-direction) of more than 15 Å to avoid spurious interaction between neighboring replicas[50]. Four ligands were connected to the gold surface via two gold adatoms. The plane-wave energy cut-off of 400 eV and Γ-centered Monkhorst-Pack grid with 0.032 Å^{-1} spacing between k-points (e.g., this is equivalent to 13×13×13 and 3×4×1 grids of the corresponding primitive cell of bulk gold *fcc* and gold-thiols $c(4\times2)$ supercells, respectively) were used to converge the total energy to < 1meV/atom; the structures were relaxed until the forces were less than 0.025 eV/Å. The computed lattice constant for bulk gold *fcc* using PBE and vdW-DF is 4.15 Å^{-1} and 4.12 Å^{-1}, respectively which values are in good agreement with other DFT calculations[42,51] and experimental value[52] of 4.078 Å^{-1}. The total energy differences ΔE between structure α (different arrangements of RS/RSOH chains with Au adatoms) and a unit cell with 4RS at bridge-*fcc* sites [4RS/Au(111)] is calculated with bulk Au as a metal atom reservoir:

$$\Delta E = E[\alpha] - E[4RS. Au(111)] - xE[Au(Bulk)]$$
$$\Delta E = E[\alpha] - E[4RSOH. Au(111)] - xE[Au(Bulk)]$$

Due to the likely metastable configurations that might describe this interface, simulated annealing along with *ab initio* molecular dynamics (AIMD) simulation was employed. Taking into account the *fcc* structure of bulk Au within the Au(111) slab, only the bottommost layer were fixed for all kinds of relaxation and simulated annealing. On the other hand—due to computational limitations—two bottommost gold layers were fixed for equilibration (4 ps) and production AIMD simulation (16 ps). AIMD simulation at 300 K of the most stable structure o(M8/C11TH) was performed to study the behavior of Au(111)/C11TH, with the *NVT* ensemble. The time step used for simulated annealing and AIMD simulation was 1 fs. **Figure S1** (*Supporting Information*) depicts the change in free energy throughout the 16 ps simulation of M8/C11TH model.

3 Results and discussion

3.1 Au (111)/SCH₃

In order to describe the atomic and electronic structure of the adsorbed thiols on the flat gold surface with saturation coverage, we considered realistic models for gold methyl thiolate proposed by Häkkinen *et al.*[14]. The gas-phase structures of various models with different orientations were obtained using both PBE and the modern vdW-DF functionals. The computed geometrical parameters and energy differences were correctly reproduced by PBE functional and vdW-DF approaches and reveals the same trends as PBE (**Table 1, Figure 1**). A considerable number of theoretical studies[19] have been done on Au (111)/SCH$_3$ without taking into account the vdW interactions. The energy differences between M8 and M9 (~0.06 eV) are small to establish stability preference for two models using PBE approach. On the other hand, the vdW-DF computed energies for M8 and M9 show that the M9 is more stable by ∼0.14 eV, with this increased stability arising due to the vdW interactions within the Au(111)/SCH$_3$ interface.
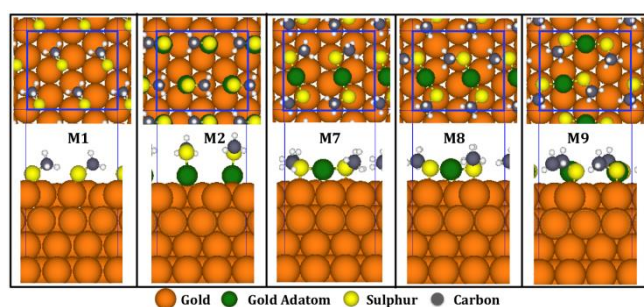

Fig. 1 DFT optimized different atomistic models for the saturation coverage of *c(4×2)* Au/CH$_3$S interface. Top panel displays the top view and the bottom panel presents the side view. Blue line indicates the unit cell.

| Model | Features | PBE | | optB86b |
		Computed	Ref.[14]	Computed
M1	(ΔE)[a], eV	0.0	0.0	0.0
	($d_{S-AuSurf}$)[b], Å	2.48	2.50	2.49
M2	(ΔE)[a], eV	+1.02	+1.28	+2.23
	($d_{S-AuSurf}$)[b], Å	2.27	2.30	2.27
M7	(ΔE)[a], eV	-0.15	-0.09	+0.09
	(d_{S-AuAd})[b], Å	2.57	2.59	2.57
	($d_{S-AuSurf}$)[c], Å	2.30	2.33	2.30
M8	(ΔE)[a], eV	-0.84	-0.78	-0.52
	(d_{S-AuAd})[b], Å	2.51	2.52	2.51
	($d_{S-AuSurf}$)[c], Å	2.31	2.34	2.32
M9	(ΔE)[a], eV	-0.90	-0.84	-0.65
	(d_{S-AuAd})[b], Å	2.51	2.52	2.51
	($d_{S-AuSurf}$)[c], Å	2.32	2.34	2.32

[a]adsorption energy obtained by PBE or vdW-DF functional per unit cell, [b]average distances between S and Au adatom and [c]average distances between S-Au Surface.

Table 1 Relative total energies, ΔE (in eV) and bond length of the DFT optimized Au/CH$_3$S interface where relative energy per *c*(4×2) unit cell is calculated with respect to M1 by using PBE and vdW-DF functional.

3.2 Au (111)/C11TH

In the following stage, the methyl thiolates were substituted by C11TH, optimized followed by simulated annealing and AIMD simulation. To explore the global minima and conformational details of any soft materials having longer chains, such as the SAMs studied here, simulated annealing or AIMD is one of the best choices. The reason is related to their amorphous like structure, as using only ionic relaxation it is difficult to obtain the global minimum structure[53]. In later sections, we will describe the simulated annealing and then AIMD simulation outcomes along with experimental observations.

To capture all possible conformations, AIMD in conjunction with simulated annealing was employed by including the vdW dispersion correction. Simulated annealing was performed for all the models with both PBE and vdW-DF. AIMD was used for the M8 by employing vdW-DF to consider the long-range dispersion. As both the M8 and M9 models have similar stability (**Table 2**), we only consider M8 as a model and compare the results with experimental observations. Simulated annealing was done in three steps: heating up to 300 K, equilibration at 300 K for 1.6 ps and cooling the system to 0 K. The final structure obtained from simulated annealing is therefore fully relaxed. The efficiency of simulated annealing depends on the cooling procedure and to obtain reliable results it is important to choose the number of ionic steps very cautiously. In this work, we used two ionic steps for the decrement of every K. This fully relaxed optimized structure obtained through annealing was then considered as the initial configurations for AIMD simulation.

3.2.1 Simulated annealing

Relative energies with and without annealing is tabulated in **Table 2**. In case of the simulation without annealing, the adsorption energy is lower with PBE level of theory than with optB86b vdW-DF. This energy difference reduces from 1.1 to 1.3 eV with the inclusion of the dispersive effects using vdW-DF by simulated annealing approach. Also, geometry obtained from simulated annealing revealed that the ligands are more inclined towards each other due to the dispersion correction for the longer alkanethiols. This is due to the attractive component of the van der Waals functional arising from the dynamical correlations between fluctuating charge distributions of the adjacent molecules[54].

Method	ΔE (eV)	M1	M7	M8	M9
wo-Annealing	PBE	0	+0.489	-0.738	-0.719
	vdW-DF	0	+0.687	-0.443	-0.471
Annealing	PBE	0	+0.236	-0.639	-0.634
	vdW-DF	0	-0.212	-1.55	-1.76

Table 2 Relative total energies, ΔE in eV, of Au(111)/ C11TH complex with and without simulated annealing of the different models with respect to M1 calculated using both PBE and vdW-DF; wo-annealing indicates adsorption energy without simulated annealing of the respective systems.

In the case of PBE, the energy difference between structures before and after annealing does not deviate significantly. This reveals that the conformation obtained from annealing are not different energetically. Observing the structure of each model in **Figure 2**, it is obvious that the chain arrangements are not identical. The chain remains straight during relaxation (*Supporting Information*, **Figure S2**) while they tried to incline to form a hydrogen bond with each other. Our calculations reveal that in case of longer alkanethiol chains, van der Waals density functionals are needed to make distinguish energetically and structurally[55,56]. The most important findings that the energy increased by vdW dispersion is rising from M7 to M9. It varies from 0.045 to 0.113 eV/CH$_2$ unit, which is on the same order of magnitude as was observed in prior experimental (≈0.08−0.04 eV/CH$_2$ unit)[7] and theoretical (≈ 0.105 eV/CH$_2$ unit) studies[42]. Little perturbation may be justified by the choice of end functional groups which are giving lower energy due to the hydrogen bonding by the –OH[53].
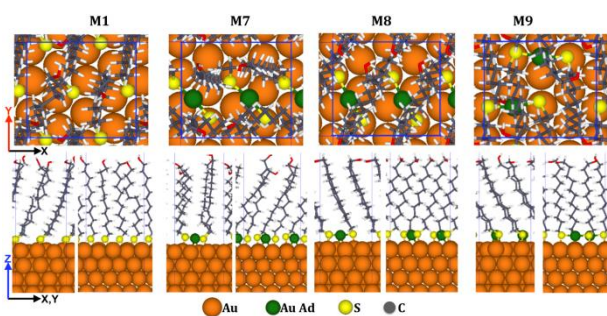

Fig 2 DFT optimized with simulated annealing different atomistic models of Au(111)/ C11TH interface using vdW density functional. Top row: top view xy plane and bottom row: side view (*xz and yz* planes).

3.2.1 AIMD simulation

Experimental evidence to characterize the Au-S bond is less prevalent for the longer chain alkanethiols since the Au-S bond is buried under the long chains. Despite a lower degree of conformational change for longer chains compare to the short one due to the weak intermolecular interaction[57], there is a chance to form different phases can arise due to the flexibility of alkyl chains[29,58].

The arrangement of C11TH SAMs can be characterized by thickness, tilt angle (θ), and azimuthal tilt angle (χ). Different experimental and molecular dynamics study[17,33,59–61] explored the SAMs process by quantifying tilt angle, tilt angle direction and the thickness of the monolayer. However, there is no concrete conclusion about what happens to the tilt angle for long alkane chains. Improving upon published results, we were able to quantify calculated parameters more accurately by using vdW dispersion correction within the AIMD approach. Due to the flexibility of the C11TH, we defined the SAM thickness as the distance vector

between the topmost atoms of C11TH (either C or O atom) and S atom of the thiol groups. We observed that the thickness of the SAMs layer changed significantly depending on the exchange functional and the sampling of ground state procedure. In simulated annealing, the thickness decreased 1.1% - 8.3% and 9.7%- 15.7% for PBE and vdW-DF, respectively. **Figure 3** shows the thickness and tilt angle of C11TH obtained from the ellipsometry and AIMD simulation. The effects of vdW-DF on thickness with simulated annealing and without simulated annealing is 0.9% - 3.1% and 3.1%- 11.6%, respectively which makes the former one more densely packed[13]. From these results, we can conclude that the van der Waals interactions give the SAMs a denser structure on the substrate. AIMD computed average thickness of C11TH for M8 is 12.9Å, which agrees with previous studies[61,62]. The experimental results obtained from ellipsometry are also in agreement as a thickness of 14.8 Å was obtained using a Cauchy layer model for C11TH (**Figure 3B**).

Another salient feature of the SAMs is tilt angle which may be defined as the angle between the surface normal (*z*-direction) and the vector passing through the S atom and the centroid of the thiols[61]. Quantification of the tilt angle is more elusive in the case of longer alkanethiols due to the flexibility of the alkane chain. To see the morphological changes for different phases, we calculate the tilt angle corresponding to S-O, S-C$_{11}$, S-C$_{10}$ vectors (*Supporting Information*, **Figure S3**). **Figure 3B** outlines the relationship between the tilt angle (S-C$_{11}$ vector) and SAM thickness of the M8 model. For other models see **Table S1** (*Supporting Information*). Although all three types of tilt angle having the same trends, the computed values can be a representation of the interaction of buried atoms and the lateral dispersion of the backbone. The flexibility of the –OH group favors the formation of hydrogen bonds between two C11THs which ensures the stability of alkanethiols on Au(111) surface and promotes saturation coverage. This phenomenon can be easily outlined from the tilt angle distribution of SO and SC11 vectors. This data indicates that the long-range interactions, such as, vdW interactions between the alkyl chains may be one of the sources for ordered SAMs surface orientation on Au(111) surface[9,63,64].
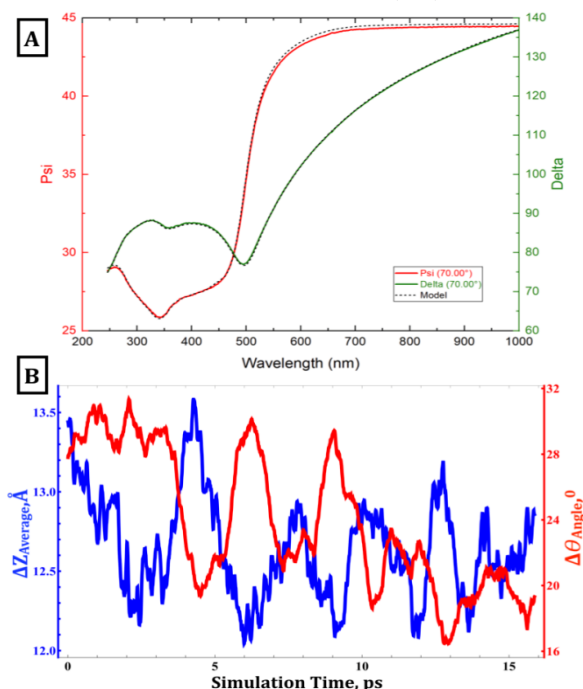
Fig 3 A) Raw variable angle psi and delta ellipsometry data collected at 70° incidence angle and fitted to a Cauchy model to determine C11TH thickness. B) Variation in thickness and tilt angle of model M8.

From the previous discussions, we have established that the tilt angle is responsible for stable orientation of thiol SAMs on Au(111) substrates. Different orientations of C11TH on $c(4×2)$ Au(111) surface is more complex because a very large number of configurations can be involved. Therefore, a detailed analysis is required to better characterize their orientation and stability. Many local minima structures exist as predicted throughout the AIMD simulation, which supports the phase transition due to longer chain orientation through Au adatom. In the case of dense SAM structures, strong steric effects originate from the chain length of longer alkanelthiolates that favors the chain to rearrange on the surface by varying tilt and azimuthal angle[30]. This arrangement allows the CH_2 unit to be flexible to minimize the vdW interaction. Accordingly, the tilt angle is the consequences of the effect of thickness.

Figure 4 represents the different orientations of the model C11TH/M8. Different orientations of alkanethiol SAMs appeared at higher coverage on the flat surface of gold[4,65]. A low-temperature STM study of thiol SAMs revealed different orientations and stabilities governed by the surface coverage, and at the saturation point the equilibrium orientation dominated over two other orientations[66]. Decanethiol[26,67] and hexanethiols[68] systems have been studied by using STM, but these efforts suggest it is not possible to capture all the molecular level changes only with experimental techniques and that molecular dynamics simulation need to be used in conjunction. The increased chain length of alkanethiols will affect vdW interaction among the chains and facilitate new structural orientations to compensate for the stability of the chains. In our study, we observed four different orientations throughout the 16 ps simulation time. Among them, three orientations such as ⟨11⟩ (33%), ⟨1̄1⟩ (31%), and ⟨01⟩ (30%) have the same contribution while ⟨10⟩ (6%) comrised only a very small portion (see **Figure S1**). The lowest energy configuration of this model is attributed to the ⟨11⟩ orientation due to the number of hydrogen bonds that form between the terminal -OH functional group of two adjacent C11TH.

Fig 4 Screenshots of different orientations obtained from a 16 ps AIMD simulation of M8/C11TH (top view). The red dotted line represents the hydrogen bonding between two adjacent –OH groups of C11TH. For clarity the hydrogen atoms are not shown with the exception of hydrogens of -OH functional group.
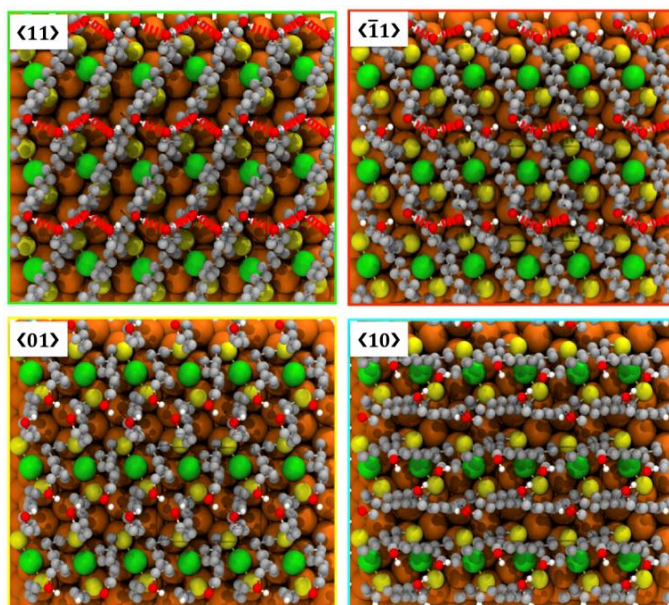
Examining the side view of the M8/C11TH orientations (*Supporting Information*, **Figure S4**), it can be inferred that the tilt angle or vdW attraction is responsible for the different degrees of stability for the SAM layer. In ⟨10⟩, the SAM layer is more extended compared to other orientations. The angle between the projected SC11 vectors of alkanethiols and *x*-axis in *xy*-plane described the tilt angle direction. The tilt angle is greatly influenced by the changes in orientations which suggest some conformational changes of the longer chains are involved. However, it is not possible to study the conformational changes of the longer chains due to the involvement of bending structures rather than straight. Definitely, a method to determine chain twist angle would enrich the understanding of the formation of different orientations, but studies become more complicated if this effect is also taken into consideration.

3.2.2 Electronic structure

To elucidate the electronic structure of Au(111)/C11TH the projected density of state (PDOS) was computed in conjunction with XPS measurements. **Figure 5** shows the computed PDOS of the different models of Au(111)/C11TH from the Au adatom to the top of the C11TH SAMs of the valence band levels. As a result, the system behaves like a semiconductor. If we go beyond the adatom, contribution coming from the other elements is fully covered by the gold due to the longer chain, and it is not possible to get the exact structure of buried Au-S interaction.
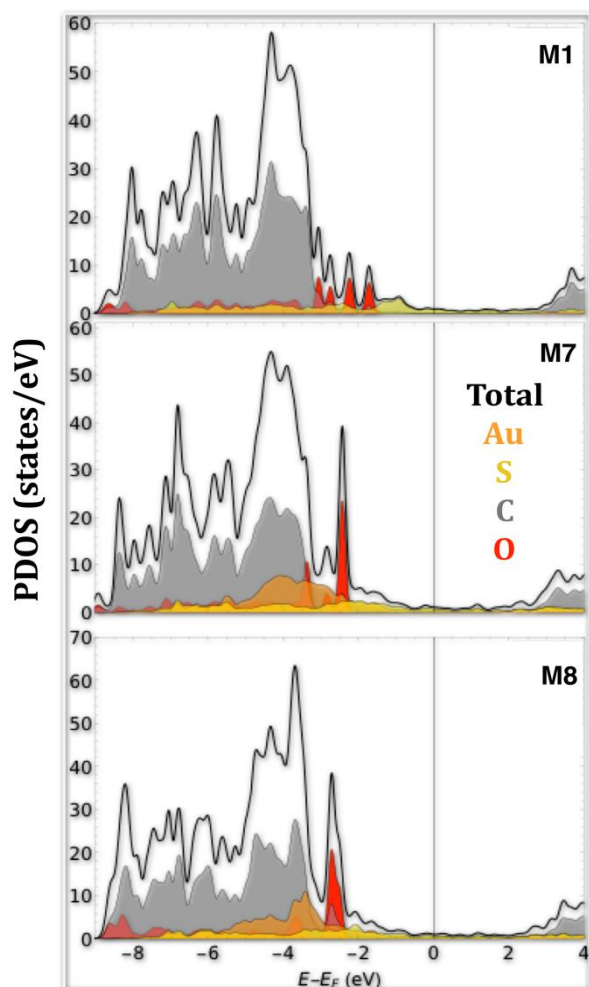
Fig 5 Computed PDOS of M1, M7 and M8/C11TH models. PDOS collected from the top C atom of C11TH up to Au adatom.

The PDOS for M1 shows four peaks around -3.5 eV to -2 eV composed of O 2p states. Apparently, in all cases C 2p states are located around -2.2 eV and the contribution of S in electronic structure is very small. But the Au 5d state of gold adatom contributes differently. This is clearer in the M8 model around -3.45 eV. Broadening and increased number of the oxygen peak is observed around -4 eV to -2 eV when one moves to the stable structure while the intensity is suppressed. **Figure 6** represents the computed weighted averaged PDOS of the configurations evolved in AIMD simulation with the subshell photoionization cross-sections and thickness of ~5.06 Å/8.75 Å (IMFP[23.5eV]/IMFP[188eV])[69-71] from the top C atom. Eventually, in this study SAMs forming ligands are not enough sturdy to form rigid structure and also the interval or duration of orientation evolution is too small. To overcome the time-lapse, we calculate the weighted averaged PDOS based on their contribution in the lifetime in each pattern.

Fig 6 DFT computed AIMD averaged PDOS of the valence band and experimental XPS spectra at two different X-ray energies: 23.5 eV (left) and 188 eV (right). (a) & (b) computed PDOS while (c) & (d) spectral modulation of the calculated

PDOS of (a) & (b) with the use of one electron and angular cross sections to the corresponding orbitals by applying IMFP at the corresponding X-ray energy. (e) & (f) are the XPS spectra. The zero point of the binding energy scale was set at the Fermi level.
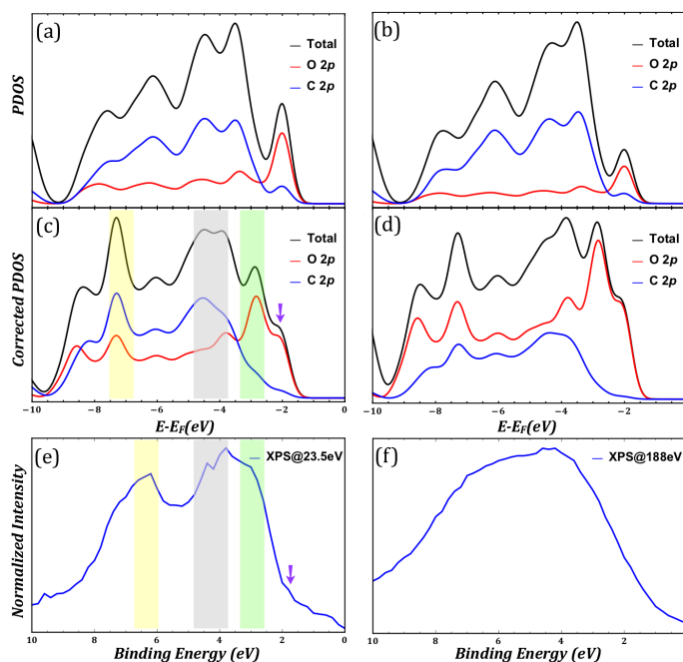
Corresponding to the X-ray energies $h\nu$=23.5 eV and 188 eV, the one-electron angular-corrected photoionization cross sections corrections have been applied to the computed averaged PDOS plots taking into account the orbital dipole asymmetry parameters[72]. Inelastic mean free path of electrons (IMFP) corresponding to the two different X-ray energies $h\nu$=23.5 eV and 188 eV was considered. From photoionization cross-section corrected data, it is observed that despite the dominance of C 2p orbitals at valence band minima (VBM), electrons would be photoemitted mainly from O 2p orbitals due to their high relative photoionization cross section. Experimentally, the signal-to-noise ratio at higher X-ray energy is improved; but the resolution is reduced (**Figures 6e and 6f**). From the AIMD we have a clear idea about how the SAMs are behaving and forming different orientations in a very small window of energy per unit cell. AIMD results provide a reliable explanation of the observed XPS.

Conclusions

We have presented a combined experimental and theoretical study that provides a molecular-level description of the SAM structure, stability of SAMs dependence on different orientations, and electronic structure of a longer chain alkanethiol, C11TH, on Au(111). In order to explore the effect of long-range correlations in this system of thiol SAMs with longer alkane chains, dispersive forces were included in a self-consistent implementation of the vdW-DF method using optB86b exchange functional. Our vdW-DF enabled AIMD simulation identified four different configurations formed by

the C11TH on Au(111) surface with different stabilities that were dependent on the hydrogen bond formation. The thickness and tilt angles distributions of the different configurations were computed and these results were compared with the experimental ellipsometry data. At higher energy (188 eV) photoionization cross section corrected PDOS revealed the prevalence of O 2p states throughout the valance band. AIMD weighted averaged DFT computed PDOS were closely correlated with the XPS results by applying the one-electron angular photoionization cross section corrected orbitals in the valence band based on the IMFP for 23.5 eV X-ray energy. These findings regarding the need to include van der Waals density functions (vdW-DF) for accurate results involving longer chain alkanes and non-alkane functional groups can be extended to understanding many other thiol-metal self-assembly interactions used in a of wide range applications.

Conflicts of interest

There are no conflicts to declare.

Acknowledgements

References

1   R. G. Nuzzo and D. L. Allara, Adsorption of bifunctional organic disulfides on gold surfaces, *J. Am. Chem. Soc.*, 1983, **105**, 4481–4483.

2   A. Ulman, Formation and Structure of Self-Assembled Monolayers, *Chem. Rev.*, 1996, **96**, 1533–1554.

3   C. Vericat, M. E. Vela, G. Corthey, E. Pensa, E. Cortés, M. H. Fonticelli, F. Ibañez, G. E. Benitez, P. Carro and R. C. Salvarezza, Self-assembled monolayers of thiolates on metals: a review article on sulfur-metal chemistry and surface structures, *RSC Adv.*, 2014, **4**, 27730.

4   F. Schreiber, Structure and growth of self-assembling monolayers, *Prog. Surf. Sci.*, 2000, **65**, 151–257.

5   B. D. Ratner, New ideas in biomaterials science--a path to engineered biomaterials., *J. Biomed. Mater. Res.*, 1993, **27**, 837–50.

6   S. Minko, in *Polymer Surfaces and Interfaces*, ed. M. Stamm, Springer Berlin Heidelberg, Berlin, Heidelberg, 2008.

7   J. C. Love, L. A. Estroff, J. K. Kriebel, R. G. Nuzzo and G. M. Whitesides, Self-assembled monolayers of thiolates on metals as a form of nanotechnology., *Chem. Rev.*, 2005,

105, 1103–69.

8   F. Tao and S. L. Bernasek, Understanding Odd−Even Effects in Organic Self-Assembled Monolayers, *Chem. Rev.*, 2007, **107**, 1408–1453.

9   S. L. Bernasek, Molecular electronics: Van der Waals rectifiers., *Nat. Nanotechnol.*, 2013, **8**, 80–1.

10   N. Nerngchamnong, L. Yuan, D.-C. Qi, J. Li, D. Thompson and C. A. Nijhuis, The role of van der Waals forces in the performance of molecular diodes., *Nat. Nanotechnol.*, 2013, **8**, 113–8.

11   S. Griessl, M. Lackinger, M. Edelwirth, M. Hietschold and W. M. Heckl, Self-Assembled Two-Dimensional Molecular Host-Guest Architectures From Trimesic Acid, *Single Mol.*, 2002, **3**, 25–31.

12   Y.-F. Liu and Y.-L. Lee, Adsorption characteristics of OH-terminated alkanethiol and arenethiol on Au(111) surfaces., *Nanoscale*, 2012, **4**, 2093–100.

13   P. Chinwangso, L. St. Hill, M. Marquez, T. Lee, P. Chinwangso, L. R. St. Hill, M. D. Marquez and T. R. Lee, Unsymmetrical Spiroalkanedithiols Having Mixed Fluorinated and Alkyl Tailgroups of Varying Length: Film Structure and Interfacial Properties, *Molecules*, 2018, **23**, 2632.

14   H. Häkkinen, The gold–sulfur interface at the nanoscale, *Nat. Chem.*, 2012, **4**, 443–455.

15   P. Maksymovych, O. Voznyy, D. B. Dougherty, D. C. Sorescu and J. T. Yates, Gold adatom as a key structural component in self-assembled monolayers of organosulfur molecules on Au(111), *Prog. Surf. Sci.*, 2010, **85**, 206–240.

16   N. B. Luque, E. Santos, J. Andres and F. Tielens, Effect of Coverage and Defects on the Adsorption of Propanethiol on Au(111) Surface: A Theoretical Study, Langmuir, 2011, 27, 14514–14521.

17   L. Strong and G. M. Whitesides, Structures of self-assembled monolayer films of organosulfur compounds adsorbed on gold single crystals: electron diffraction studies, *Langmuir*, 1988, **4**, 546–558.

18   R. G. Nuzzo, B. R. Zegarski and L. H. Dubois, Fundamental studies of the chemisorption of organosulfur compounds on gold(111). Implications for molecular self-assembly on gold surfaces, *J. Am. Chem. Soc.*, 1987, **109**, 733–740.

19   Q. Guo and F. Li, Self-assembled alkanethiol monolayers on gold surfaces: resolving the complex structure at the interface by STM., *Phys. Chem. Chem. Phys.*, 2014, **16**, 19074–19090.

20   P. O. Bedolla, G. Feldbauer, M. Wolloch, S. J. Eder, N. Dörr, P. Mohn, J. Redinger and A. Vernes, Effects of van der Waals interactions in the adsorption of isooctane and ethanol on Fe(100) surfaces, *J. Phys. Chem. C*, 2014, **118**, 17608–17615.

21   N. Ferri, R. A. DiStasio, A. Ambrosetti, R. Car and A. Tkatchenko, Electronic Properties of Molecules and Surfaces with a Self-Consistent Interatomic van der Waals Density Functional, *Phys. Rev. Lett.*, 2015, **114**, 176802.

22   J. L. ;Jonatha. W. S. Atweood, Ed., *Encyclopedia of*

supramolecular chemistry, Marcel Dekhar Inc., 2004.

23   L. Yang, C. Adam, G. S. Nichol and S. L. Cockroft, How much do van der Waals dispersion forces contribute to molecular recognition in solution?, *Nat. Chem.*, 2013, **5**, 1006–10.

24   H. Zhao, S. Zhang, S. Li, X. Song, W. Liu, B. Liu and M. Dong, Investigation of the non-covalent interactions of molecular self-assembly by scanning tunneling microscopy using the association of aromatic structures in pyrene-4,5,9,10-tetraone and phenanthrene-9,10-dione molecules, *RSC Adv.*, 2015, **5**, 103316–103320.

25   D. Nassoko, M. Seydou, C. Goldmann, C. Chanéac, C. Sanchez, D. Portehault and F. Tielens, Rationalizing the formation of binary mixed thiol self-assembled monolayers, Mater. Today Chem., 2017, 5, 34–42.

26   Y. Qian, G. Yang, J. Yu, T. A. Jung and G. Liu, Structures of Annealed Decanethiol Self-Assembled Monolayers on Au(111): an Ultrahigh Vacuum Scanning Tunneling Microscopy Study, *Langmuir*, 2003, **19**, 6056–6065.

27   M. J. Esplandiú, H. Hagenström and D. M. Kolb, Functionalized Self-Assembled Alkanethiol Monolayers on Au(111) Electrodes: 1. Surface Structure and Electrochemistry, *Langmuir*, 2001, **17**, 828–838.

28   H. Grönbeck, H. Häkkinen and R. L. Whetten, Gold - Thiolate Complexes Form a Unique c (4 × 2) Structure on Au (111), *J. Phys. Chem. C*, 2008, 15940–15942.

29   H. Grönbeck, A. Curioni and W. Andreoni, Thiols and Disulfides on the Au(111) Surface: The Headgroup−Gold Interaction, *J. Am. Chem. Soc.*, 2000, **122**, 3839–3842.

30   Y. Cao, Q. Ge, D. J. Dyer and L. Wang, Steric Effects on the Adsorption of Alkylthiolate Self-Assembled Monolayers on Au (111) †, *J. Phys. Chem. B*, 2003, **107**, 3803–3807.

31   H. Guesmi, N. B. Luque, E. Santos and F. Tielens, Does the S−H Bond Always Break after Adsorption of an Alkylthiol on Au(111)?, Chem. - A Eur. J., 2017, 23, 1402–1408.

32   F. Tielens and E. Santos, AuS and SH Bond Formation/Breaking during the Formation of Alkanethiol SAMs on Au(111): A Theoretical Study, *J. Phys. Chem. C*, 2010, **114**, 9444–9452.

33   Y. Y. Yimer, K. C. Jha and M. Tsige, Epitaxial transfer through end-group coordination modulates the odd-even effect in an alkanethiol monolayer assembly., *Nanoscale*, 2014, **6**, 3496–502.

34   S. Franzen, Density functional calculation of a potential energy surface for alkane thiols on Au(111) as function of alkane chain length, *Chem. Phys. Lett.*, 2003, **381**, 315–321.

35   D. Fischer, A. Curioni and W. Andreoni, Decanethiols on Gold: The Structure of Self-Assembled Monolayers Unraveled with Computer Simulations, *Langmuir*, 2003, **19**, 3567–3571.

36   F. P. Cometto, P. Paredes-Olivera, V. A. Macagno and E. M. Patrito, Density functional theory study of the adsorption of alkanethiols on Cu(111), Ag(111), and Au(111) in the low and high coverage regimes., *J. Phys. Chem. B*, 2005, **109**, 21737–48.

37   E. Torres, A. T. Blumenau and P. U. Biedermann, Steric and chain length effects in the (√(3)×√(3))R30° structures of alkanethiol self-assembled monolayers on Au(111)., *Chemphyschem*, 2011, **12**, 999–1009.

38   J. L. C. Fajín, F. Teixeira, J. R. B. Gomes and M. N. D. S. Cordeiro, Effect of van der Waals interactions in the DFT description of self-assembled monolayers of thiols on gold, *Theor. Chem. Acc.*, 2015, **134**, 67.

39   L. Ferrighi, Y. Pan, H. Grönbeck and B. Hammer, Study of Alkylthiolate Self-Assembled Monolayers on Au(111) Using a Semilocal meta-GGA Density Functional, *J. Phys. Chem. C*, 2012, **116**, 7374–7379.

40   A. H.-T. Li and S. D. Chao, Intermolecular potentials of the methane dimer calculated with Møller-Plesset perturbation theory and density functional theory., *J. Chem. Phys.*, 2006, **125**, 094312.

41   S. Tsuzuki and H. P. Lüthi, Interaction energies of van der Waals and hydrogen bonded systems calculated using density functional theory: Assessing the PW91 model, *J. Chem. Phys.*, 2001, **114**, 3949.

42   P. Carro, E. Pensa, C. Vericat and R. C. Salvarezza, Hydrocarbon Chain Length Induces Surface Structure Transitions in Alkanethiolate–Gold Adatom Self-Assembled Monolayers on Au(111), *J. Phys. Chem. C*, 2013, **117**, 2160–2165.

43   G. Kresse and J. Furthmüller, Efficiency of ab-initio total energy calculations for metals and semiconductors using a plane-wave basis set, *Comput. Mater. Sci.*, 1996, **6**, 15–50.

44   G. Kresse and J. Hafner, Ab initio molecular-dynamics simulation of the liquid-metal–amorphous-semiconductor transition in germanium., *Phys. Rev. B*, 1994, **49**, 14251–14269.

45   J. P. Perdew, K. Burke and M. Ernzerhof, Generalized Gradient Approximation Made Simple, *Phys. Rev. Lett.*, 1996, **77**, 3865–3868.

46   M. Dion, H. Rydberg, E. Schröder, D. C. Langreth and B. I. Lundqvist, Van der Waals Density Functional for General Geometries, *Phys. Rev. Lett.*, 2004, **92**, 246401.

47   J. Klimeš, D. R. Bowler and A. Michaelides, Van der Waals density functionals applied to solids, *Phys. Rev. B*, 2011, **83**, 195131.

48   G. Kresse, From ultrasoft pseudopotentials to the projector augmented-wave method, *Phys. Rev. B*, 1999, **59**, 1758–1775.

49   C. Vericat, M. E. Vela, G. a Benitez, J. a M. Gago, X. Torrelles and R. C. Salvarezza, Surface characterization of sulfur and alkanethiol self-assembled monolayers on Au(111), *J. Phys. Condens. Matter*, 2006, **18**, R867–R900.

50   Y. Wang, Q. Chi, N. S. Hush, J. R. Reimers, J. Zhang and J. Ulstrup, Gold Mining by Alkanethiol Radicals: Vacancies and Pits in the Self-Assembled Monolayers of 1-Propanethiol and 1-Butanethiol on Au(111), *J. Phys. Chem. C*, 2011, **115**, 10630–10639.

51   T. T. Järvi, a. Kuronen, M. Hakala, K. Nordlund, a. C. T. Van Duin, W. a. Goddard and T. Jacob, Development of a ReaxFF description for gold, *Eur. Phys. J. B*, 2008, **66**, 75–

79.

52   W. Pearson, *A handbook of lattice spacings and structures of metals and alloys.*, Pergamon Press, New York, 1958.

53   F. Tielens, D. Costa, V. Humblot and C.-M. Pradier, Characterization of ω-Functionalized Undecanethiol Mixed Self-Assembled Monolayers on Au(111): A Combined Polarization Modulation Infrared Reflection−Absorption Spectroscopy/X-ray Photoelectron Spectroscopy/Periodic Density Functional Theory Study, *J. Phys. Chem. C*, 2008, **112**, 182–190.

54   F. London, Uber einige Eigenschaften und Anwendungen der Molekularkraﬁte, *Z. Phys. Chem.*, 1930, 222–251.

55   E. Mete, A. Yılmaz and M. F. Danışman, A van der Waals density functional investigation of carboranethiol self-assembled monolayers on Au(111), *Phys. Chem. Chem. Phys.*, 2016, **18**, 12920–12927.

56   R. C. Salvarezza and P. Carro, The electrochemical stability of thiols on gold surfaces, *J. Electroanal. Chem.*, 2018, **819**, 234–239.

57   E. Bedford, V. Humblot, C. Méthivier, C.-M. Pradier, F. Gu, F. Tielens and S. Boujday, An Experimental and Theoretical Approach to Investigate the Effect of Chain Length on Aminothiol Adsorption and Assembly on Gold., *Chemistry*, 2015, **21**, 14555–61.

58   V. Velachi, D. Bhandary, J. K. Singh and M. N. D. S. Cordeiro, Structure of Mixed Self-Assembled Monolayers on Gold Nanoparticles at Three Different Arrangements, *J. Phys. Chem. C*, 2015, **119**, 3199–3209.

59   a Cossaro, R. Mazzarello, R. Rousseau, L. Casalis, A. Verdini, A. Kohlmeyer, L. Floreano, S. Scandolo, A. Morgante, M. L. Klein and G. Scoles, X-ray diffraction and computation yield the structure of alkanethiols on gold(111)., *Science*, 2008, **321**, 943–946.

60   R. G. Nuzzo, L. H. Dubois and D. L. Allara, Fundamental studies of microscopic wetting on organic surfaces. 1. Formation and structural characterization of a self-consistent series of polyfunctional organic monolayers, *J. Am. Chem. Soc.*, 1990, **112**, 558–569.

61   V. Vasumathi and M. N. D. S. Cordeiro, Molecular dynamics study of mixed alkanethiols covering a gold surface at three different arrangements, *Chem. Phys. Lett.*, 2014, **600**, 79–86.

62   M. D. Porter, T. B. Bright, D. L. Allara and C. E. D. Chidsey, Spontaneously Organized Molecular Assemblies. 4. Structural Characterization of n-Alkyl Thiol Monolayers on Gold by Optical Ellipsometry, Infrared Spetcroscopy, and Electrochemistry, *J. Am. Chem. Soc.*, 1987, **109**, 3559–3568.

63   M. Amit, S. Yuran, E. Gazit, M. Reches and N. Ashkenasy, Tailor-Made Functional Peptide Self-Assembling Nanostructures, Adv. Mater., 2018, 30, 1707083.

64   Z. Li, K. Munro, M. R. Narouz, A. Lau, H. Hao, C. M. Crudden and J. Hugh Horton, Self-Assembled N-Heterocyclic Carbene-Based Carboxymethylated Dextran Monolayers on Gold as a Tunable Platform for Designing Affinity-Capture Biosensor Surfaces, ACS Appl. Mater. & Interfaces, 2018, 10, 17560–17570.

65   F. Li, L. Tang, O. Voznyy, J. Gao and Q. Guo, The striped phases of ethylthiolate monolayers on the Au(111) surface: a scanning tunneling microscopy study., *J. Chem. Phys.*, 2013, **138**, 194707.

66   G. E. Poirier, Coverage-Dependent Phases and Phase Stability of Decanethiol on Au(111), *Langmuir*, 1999, **15**, 1167–1175.

67   M. Toerker, R. Staub, T. Fritz, T. Schmitz-Hübsch, F. Sellam and K. Leo, Annealed decanethiol monolayers on Au(111) – intermediate phases between structures with high and low molecular surface density, *Surf. Sci.*, 2000, **445**, 100–108.

68   L. H. Dubois, B. R. Zegarski and R. G. Nuzzo, Molecular ordering of organosulfur compounds on Au(111) and Au(100): Adsorption from solution and in ultrahigh vacuum, *J. Chem. Phys.*, 1993, **98**, 678.

69   S. Tanuma, C. J. Powell and D. R. Penn, Calculations of Electron Inelastic Mean Free Paths., *Surf. interface Anal.*, 2000, **21**, 165–176.

70   C. J. Powell and A. Jablonski, Evaluation of Calculated and Measured Electron Inelastic Mean Free Paths Near Solid Surfaces, *J. Phys. Chem. Ref. Data*, 1999, **28**, 19.

71   M. P. Seah and W. a. Dench, Quantitative electron spectroscopy of surfaces: A standard data base for electron inelastic mean free paths in solids, *Surf. Interface Anal.*, 1979, **1**, 2–11.

72   J. J. Yeh and I. Lindau, Atomic subshell photoionization cross sections and asymmetry parameters: $1 \leqslant Z \leqslant 103$, *At. Data Nucl. Data Tables*, 1985, **32**, 1–155.